Title

Design and optimization of an air distributor for an almond stockpile heated and ambient air dryer (SHAD) - Part 1

Authors

Mayanja, Ismael K

Donis-González, Irwin R

Publication Date

2023-11-01

DOI

10.1016/j.biosystemseng.2023.10.002

Available online at www.sciencedirect.com

ScienceDirect

journal homepage: www.elsevier.com/locate/issn/15375110

Research Paper

Design and optimization of an air distributor for an almond stockpile heated and ambient air dryer (SHAD) - Part 1

Ismael K. Mayanja, Irwin R. Donis-González *

Department of Biological and Agricultural Engineering, University of California Davis, One Shields Avenue, Davis, CA 95616, USA

ARTICLE INFO

Article history:
Received 22 March 2023
Received in revised form
27 September 2023
Accepted 3 October 2023

Keywords:
Airflow
Optimization
CFD
Stockpile
Cone-shape
Multiple outlets

A stockpile heated and ambient air dryer (SHAD) was developed as an alternative to conventional almond windrow drying. Previous experiments showe that the drying air produced by SHAD was undesirably distributed through the almond stockpile. Therefore, an air distributor was developed containing 12 outlets, arranged in 4 rows of 3 outlets each. This study describes the comprehensive process of the air distributor design, manufacturing, and its optimization. The optimization process employed both computational fluid dynamics simulations and in-field airflow validation measurements. Initial 4-row air distributor in-field validation measurements indicated airflow distribution percentages were 4.1%, 30.8%, 44.9%, and 20.2% for the outlets in rows 1 through 4. This showed that almonds located around row 1 would not receive sufficient air to properly dry. Thus, an optimized 3-row air distributor configuration was developed and validated to yield an airflow distribution percentage of 31.3%, 44.4%, and 24.3% for outlets in the second to fourth rows, respectively. The 3-row air distributor configuration is therefore desirable, as the middle and tallest section of the stockpile will receive the highest airflow. The air distributor therefore markedly enhanced the SHAD's air supply distribution.

1. Introduction

Conventional windrow drying of almonds is prone to pest and human pathogen infestation (Schatzki & Ong, 2001; Martha et al., 2012). It affects timely irrigation (Goldhamer & Viveros, 2002) and involves harvesting steps, such as picking and sweeping, which generate significant and undesirable dust (CARB, 2017; Downey et al., 2008). To address these challenges, a previous study by Mayanja et al. (2021) developed and evaluated the performance of a dryer to dehydrate almonds in a stockpile referred to as a "stockpile heated and ambient air dryer (SHAD)". The purpose of the SHAD was to facilitate timely irrigation and eliminate the existing harvesting dust-generating steps such as picking and sweeping. However, the SHAD did not properly distribute the drying air within the almond stockpile, consequently leading to uneven drying. Additionally, the coefficient of performance (COP) of the SHAD was 1.33, which was above the limits of other commercially available dryers (Mayanja et al., 2021), suggesting that the drying air was not efficiently used to dehydrate the almonds within the stockpile. Hence, it was considered imperative to

* *Corresponding author.*
E-mail address: irdonisgon@ucdavis.edu (I.R. Donis-González).
https://doi.org/10.1016/j.biosystemseng.2023.10.002

Nomenclature

Abbreviations

CFD	Computational fluid dynamics
COP	Coefficient of performance
SHAD	Stockpile heated and ambient air dryer

Symbols

A	Area of pipe (m^2)
h	Specific enthalpy (J kg^{-1})
m	Molar mass (kg mol^{-1})
n	Number of moles
N	Number of outlets
θ	Angle of outlet (°)
P	Pressure (Pa)
Pv	Velocity pressure (Pa)
Q	Airflow (m^3 s^{-1})
R	Gas constant (J K^{-1} mol^{-1})
RMSE %	Root mean square error (%)
SD	Standard deviation
S_E	Energy Source (kg m^{-1} s^3)
S_M	Momentum source (kg m^{-2} s^{-2})
T	Air temperature (K)
t	Time (s)
U	Fluid velocity (m s^{-1})
V	Airspeed at outlet (m s^{-1})
x	Vertical distance from divider (m)
y	Longitudinal distance from divider (m)
β	Airflow distribution (%)
λ	Fluid thermal conductivity (W m^{-1} K^{-1})
μ	Fluid dynamic viscosity (mPa s)
ρ	Density of air (kg m^{-3})

develop an air distributor to enhance the distribution of the drying air throughout the almond stockpile.

Airflow distribution is characterized by the movement of air from regions of high to low pressure (RSES, 2008). Airflow is bound by three fundamental conservation laws of physics (Cengel & Cimbala, 2017): *1) mass*, which states that the mass of air can neither be created nor destroyed; *2) energy*, which states that the sum of all energy types (kinetic, potential, and internal) along the air stream is the same at every point; and *3) momentum*, which states that air movement can only be induced by an external force, such as a fan in the case of the SHAD. The mass, momentum, and energy conservation laws are described by the Navier–Stokes differential equations as shown in Eqs. (1)–(3). Additionally, airflow is mainly categorized into laminar or turbulent flows (Riveros & Riveros-Rosas, 2010). Their derivation and boundary condition definitions are described by Drazin and Riley (2006).

$$\frac{\partial \rho}{\partial t} + \nabla .\ (\rho U) = 0 \tag{1}$$

$$\frac{\partial \rho U}{\partial t} + \nabla .\ (\rho U \times U) = \nabla .\ \{ -p\delta + \mu \left[\nabla U + (\nabla U)^T \right] \} + S_M \tag{2}$$

$$\frac{\partial \rho h}{\partial t} + \nabla .\ (\rho U h) = \nabla .\ (\lambda \nabla T) + S_E \tag{3}$$

where, ρ is air density (kg m^{-3}) with a value of 1.204 kg m^{-3}, U is air velocity vector (m s^{-1}), μ is dynamic air viscosity (mPa s) with a value of 0.01825 mPa s, S_M is momentum source (kg m^{-2} s^{-2}), h is specific static enthalpy (J kg^{-1}), λ is air thermal conductivity (W m^{-1} K^{-1}) with a value of 0.02514 W m^{-1} K^{-1} and S_E is energy source (kg m^{-1} s^3).

Air distribution systems play a crucial role in dryer design to facilitate the uniform distribution of the heated or ambient drying air, ensuring consistent food drying. Also, the ventilation industry adopts the use of air distributors to optimize room heating and cooling (Awbi, 1998; Nielsen, 2015). A typical air distributor consists of a plenum chamber, which reduces the turbulence of the inlet air flow, before splitting it into multiple outlets; and outlets (air ducts, perforations, false floors), which are the drying air exit points aimed at removing moisture from the foods (Versteeg & Malalasekera, 2007).

Designing an optimized system to efficiently distribute the air from the SHAD to almond stockpiles could be a complex, time-consuming, and costly process. However, these challenges can be mitigated through the application of computational fluid dynamics (CFD) techniques. Various experimental and numerical studies have employed CFD to analyze and improve air distribution in different applications and designs such as a three-lateral dividing manifold (Hassan et al., 2015), a fluidized bed equipment (Depypere & Dewettinck, 2004), and also a hydrogen reformer furnace (Zhou et al., 2009). To the best of our knowledge, air distributors have not been developed as an addition for stockpile drying, including almonds. Therefore, in this study, an air distributor comprising 12 outlets using both vertical and horizontal air distribution was fabricated from a CFD model, as an addition to the SHAD. The air distributor was placed within the SHAD A-frame, underneath the almond stockpile. Hence, the primary objective of this study was the modeling, designing, fabrication, validation, and optimization of a multi-outlet SHAD air distributor. The practical application and effect on energy consumption, drying, and almond quality are described in part 2 of this study (Mayanja et al., 2023).

2. Materials and methods

2.1. Air distributor design and CFD modeling

The three-dimensional (3D) CFD model design and simulations of the SHAD air distributor were performed in SolidWorks 2019 Service Pack (SP) 3.0 and its CFD simulation tool (Dassault Systèmes SolidWorks Corp, Waltham, MA, USA). The air distributor for the SHAD was categorized into two main components, the plenum chamber and the divider.

2.1.1. Plenum chamber

The plenum chamber was directly connected to the fan, which was intended to uniformly distribute the drying air through the outlets to the almond stockpile. Its key role is to produce a uniform airflow to achieve a similar pressure and temperature

(T) along its length before subsequently diffusing the drying air by the outlets (IRRI, 2021). There are two main designs of plenum chamber, an extended chamber, which contains a main large duct with multiple outlets along its cross-section; and radial plenum, which does not contain a main duct, but rather has individual outlets connected to the main air supply or fan. In this study, an extended plenum with a cuboid cross-sectional shape was used, since this design allows for a higher airflow rate distribution with reduced airflow resistance through multiple outlets (Cengel & Cimbala, 2017). Three main shapes of outlets, including round, square, and rectangular can be used. Round outlets were used in this study as this type offers the least resistance along the longitudinal air path, requiring less fan power, using the least amount of material, and producing lower frequency noise (IRRI, 2021). Twelve outlets in 4 rows with 3 on each side (left, right, and top) were placed on the plenum, as represented in Fig. 1a.

2.1.2. *Divider*

When air is forced through a uniform cuboid cross-section plenum chamber, as seen in Fig. 1b, air velocity pressure increases along the longitudinal path, therefore forcing the majority of the air through the outlets furthest to the air inlet, or fan (IRRI, 2021). This results in insufficient airflow distribution to the outlets closer to the air inlet (Jones, 2019). To rectify this issue, a tapered plenum chamber was added, as shown in Fig. 1c (Hassan et al., 2014), since this could yield a more uniform air distribution across multiple outlets by creating an inverse relationship between the exerted velocity pressure and the area within the plenum chamber (Cengel & Cimbala, 2017). Therefore, a three-sided tapered divider was placed inside the air distributor plenum chamber to gradually increase the pressure of the air through its longitudinal path, as shown in Fig. 2, thus improving the air distribution through the outlets.

2.1.3. *CFD simulation*

CFD simulations are typically categorized into internal and external analyses. The internal analysis includes airflow within the air distributor model or the path of the drying air from the fan to the outlets. Conversely, external analysis pertains to the airflow surrounding the CFD model (Matsson, 2012). In this study, external analysis was not considered as the air distributor is engulfed by the almond stockpile. The inlet airflow of 1.2 $m^3 s^{-1}$, equivalent to the airflow provided by the fan, and a static atmospheric pressure of 101,325 Pa were considered to simulate an open environment model (Matsson, 2012). Then, the CFD simulation was conducted and the volume flow rate for each of the 12 outlets was output and recorded.

The estimation of the air distributor dimensions was based on fixed and variable parameters. Fixed parameters were selected based on space constraints, applicability, and design feasibility. Fixed parameters included: 1) The overall air distributor length of 3 m long (including outlets) to dry typically sized stockpiles with a width of 0.5 m based on the available space within the SHAD A-frame; 2) Outlet dimensions, which were 0.1 m diameter, 0.1 m length, and 0.6 m spacing from each

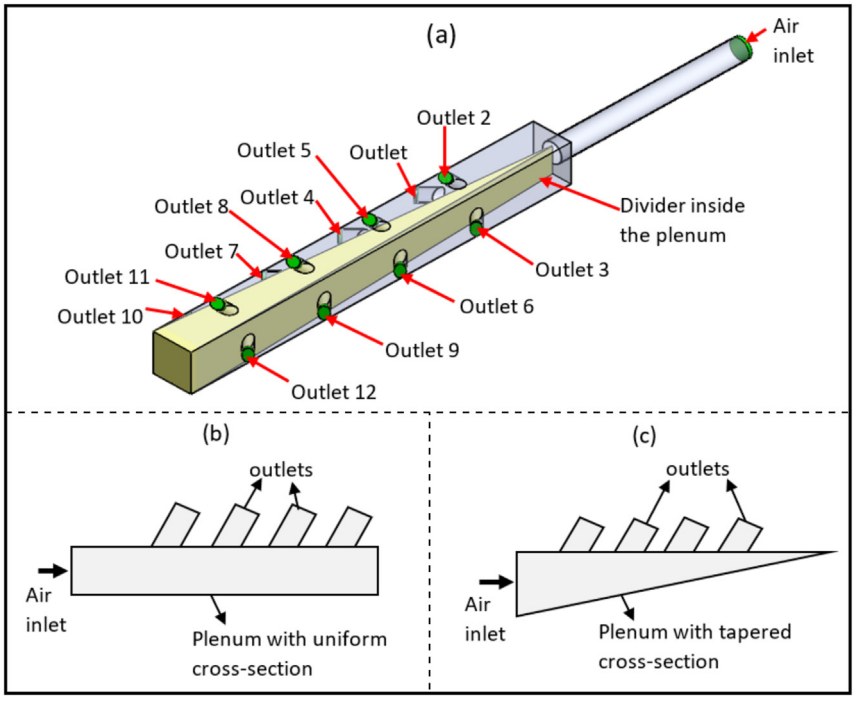

Fig. 1 – (a) 3D design of the air distributor showing the outlets numbered from 1 to 12 (grouped in 4 rows), and placement of the divider inside the plenum. Colour reference (Green for outlets and inlet, grey for the plenum, and yellow for the divider), Schematic representation of: (b) plenum with uniform longitudinal cross-section, and (c) plenum with tapered longitudinal cross-section. (For interpretation of the references to colour in this figure legend, the reader is referred to the Web version of this article.)

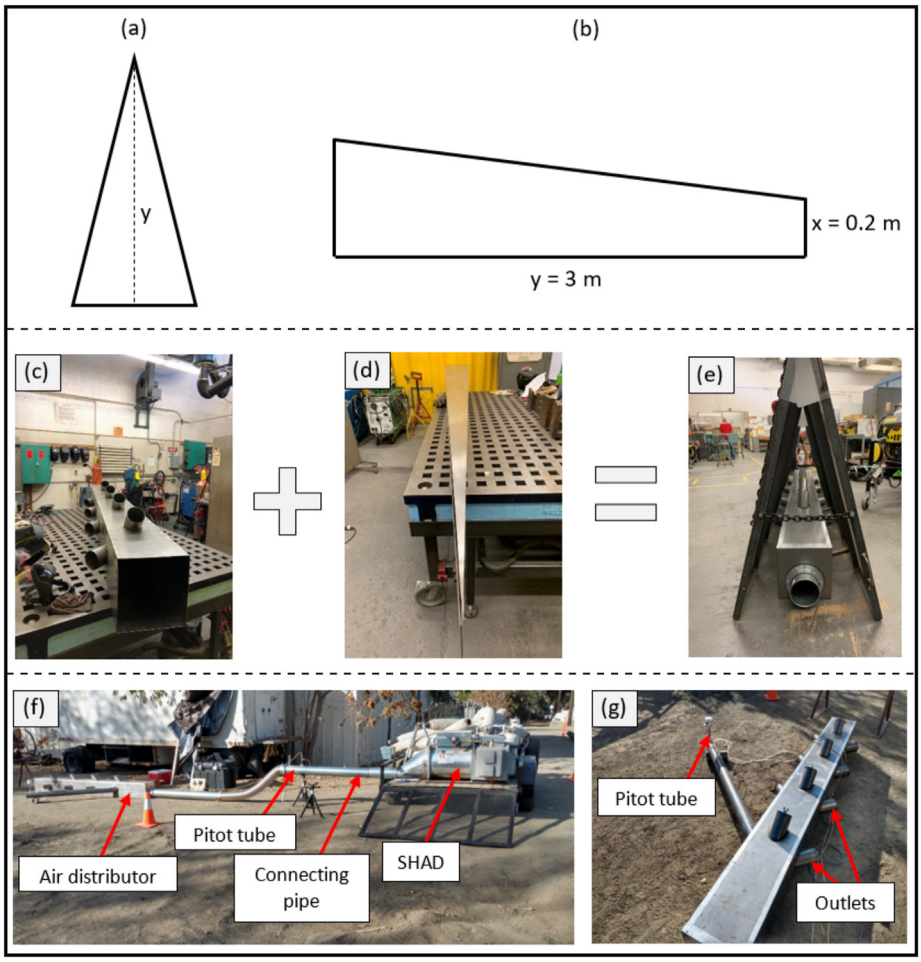

Fig. 2 – Schematic representation of the divider showing the: (a) top, and (b) side views. Picture showing: (c) plenum, (d) divider, (e) air distributor 'assembly' (plenum chamber and divider) placed within the SHAD A-frame, (f) in-field airflow measurement set-up, and (g) air distributor showing the outlet pitot tube.

other, sufficient to cover the length of the plenum chamber. Variable parameters were optimized to provide the lowest deviation between the outlets' airflow, including: 1) Outlet angle of inclination (θ); 2) longitudinal distance from both ends of the divider (y) (Fig. 2a); and 3) vertical distance from the front end of the divider (x) (Fig. 2b). The air distributor with $\theta = 45°$, $y = 3$ m, and $x = 0.2$ m showed the lowest standard deviation of airflow between outlets, as seen in Table 1.

Table 1 – Air distributor variable parameters. ✗ indicates a rejected parameter shows an accepted parameter. Accepted parameters were considered to create the initial 4-row configuration design.

Outlet angle of inclination (θ °)	30	45	60	70	90	
	✗	✓	✗	✗	✗	
Divider Height (x m)	0.17	0.18	0.19	0.2	0.21	0.22
	✗	✗	✗	✓	✗	✗
Divider Length (y m)	2.5	2.6	2.7	2.8	2.9	3.0
	✗	✗	✗	✗	✗	✓

2.2. *Air distributor fabrication*

The air distributor (Fig. 2c, d, and e), comprising the plenum and divider, was manufactured at the University of California, Davis, Biological and Agricultural Engineering (BAE) manufacturing shop, from 18 GA carbon steel metal sheets.

2.3. *In-field airflow measurements*

The air distributor was connected to the SHAD in an open outdoor space to measure the airflow in each outlet. The SHAD consisted of a 1.49 kW propane-heated vane axial fan with a 457.2 mm diameter outlet (Sukup Manufacturing Co, Sheffield, IA, USA). The fan was powered by a 12-kW generator (Model 100297, Champion Global Power Equipment, Santa Fe Springs, CA, USA). Two straight 304 stainless steel ducts of 152.4 mm diameter, 1.5 m length, and one 152.4 mm diameter 304 stainless steel hose were used to connect the outlet of the SHAD's fan to the inlet of the air distributor, as shown in Fig. 2f.

One Pitot tube (DS 300 flow sensors, Dwyer Instrument Inc, Michigan City, IN, USA) was inserted in a 0.15 m pipe connecting the outlet of the fan to the air distributor, 2.2 m away from the fan to measure inlet airflow under approximate laminar flow (Cengel & Cimbala, 2017). A second pitot tube

(PAFS-1010 flow sensors, Dwyer Instrument Inc, Michigan City, IN, USA) was inserted into a 0.1 m pipe connected to the air distributor outlets, 2.4 m away from the output of each outlet to measure the airflow per outlet, as shown in Fig. 2g. A pressure sensor (Series MS Magnesense, Dwyer Instruments Inc, Michigan City, IN, USA) was connected to each of the pitot tubes to record the static and total pressure at 5 s intervals. The difference between total and static pressures yields the velocity pressure (Pv). Airflow (Q) was calculated in $m^3\ s^{-1}$ using Eqs. (4) and (5) (Cengel & Cimbala, 2017).

$$V = \sqrt{\frac{2P_v}{\rho}} \tag{4}$$

$$Q = AV \tag{5}$$

where V is airspeed ($m\ s^{-1}$), and A the area (0.008 m^2) for the inlet pipe and each of the outlets, respectively.

An average heated drying T of 55.4 °C and ambient drying T of 16.7 °C measured by an embedded T sensor (HX94C, Omega Engineering Inc, Norwalk, CT, USA) were used to calculate the density of air (ρ), as stated in Eq. (6) (Dickerson et al., 1979).

$$\rho = \frac{P\ m}{n\ R\ T} \tag{6}$$

where P is atmospheric pressure (101,325 Pa), m is air molar mass (0.02896 kg mol^{-1}), n is number of moles (taken as 1 to match units of molar mass) and R gas constant (8.3145 J K^{-1} mol^{-1}).

The percentage airflow distribution (β) was calculated using Eq. (7) (Hassan et al., 2014), reflecting the airflow per outlet, or group of outlets, in relation to the inlet airflow.

$$\beta = \frac{Q_i}{Q}100 \tag{7}$$

where i is outlet number, β is flow ratio for the ith outlet, Q_i is air flow rate of the ith outlet ($m^3\ s^{-1}$) and Q is inlet airflow ($m^3\ s^{-1}$).

2.4. Air distribution optimization

The air distributor was optimized by determining the ideal air distributor configuration to match the natural shape of an almond stockpile. The essence of an optimized air distributor lies in its capacity to efficiently distribute air across outlets, aligning with a predefined airflow requirement per outlet. Optimization was performed by evaluating the changes in air distribution through subsequent sealing of outlets in Rows 1 through 4 with 152.4 mm diameter wingnut expansion plugs (McMaster-Carr Supply co, Santa Fe Springs, CA). Outlets in a sealed row that generated the lowest airflow standard deviation (SD) were calculated using Eq. (8), in relationship to unsealed outlets considered in the optimized design (Leys et al., 2013; Wan et al., 2014).

$$SD = \sqrt{\frac{\sum Q_i^2 - \frac{\left(\sum Q_i\right)^2}{N}}{N-1}} \tag{8}$$

where n is the total number of open outlets ($N = 9$).

Most air distribution systems, such as building ventilation units (Lin et al., 2005), parallel flow heat exchangers (Camilleri et al., 2015; Wang et al., 2011), tray dryers (Colak & Hepbasli, 2007), and bin dryers (Tórrez et al., 1998), focus on delivering equal airflow quantities through each outlet. However, optimising the air distributor for the SHAD must consider the natural conical shape of the almond stockpile, which results from how the conveyor cart deposits the almonds to form a stockpile. This means that an optimized design has to deliver the most air to the outlets in the middle region (rows 2 and 3) of the stockpile, as this is where most of the almonds in the stockpile are located.

2.5. CFD air distributor model validation

The CFD model validation for the 4-row and 3-row optimized air distributor configurations was performed by determining the variation between the in-field and CFD outlet airflow data, expressed as the percentage root mean square error (RMSE %), as shown in Eq. (9) (Royapoor & Roskilly, 2015; Lee et al., 2020)

$$RMSE\% = \frac{\sqrt{\sum_{i=1}^{N}\frac{(M_i - S_i)^2}{N_i}}}{\frac{1}{N}\sum_{i=1}^{N} M_i} \times 100 \tag{9}$$

where i is outlet number, N is total number of outlets (12), S_i is predicted CFD airflow for the ith outlet, M_i is measured in-field airflow for the ith outlet.

3. Results and discussion

3.1. Divider design based on the CFD model

Figures 3a and b include the surface plots showing the velocity pressure distribution within the plenum with and without the divider, respectively. The novelty of this design is its implementation of a three-sided divider to establish a three-directional tapered plenum in relationship to its twelve outlets. Consequently, the velocity pressure inversely changes along the path of plenum chamber (Cengel & Cimbala, 2017) producing dissimilar airflows at the outlets (Daly, 2002). A similar principle was applied by Hassan et (2014) to design a five-outlet tapered water distribution manifold.

3.2. In-field airflow measurements and CFD air distributor model validation for the initial 4-row configuration

Figure 4a shows the in-field airflow measurement results (black line) and corresponding β-values (grey bars) when all the outlets are open in the initial 4-row air distributor configuration. Row 1 (outlets 1–3) yielded the lowest β-value of 4.1%. A low average β-value for outlets in Row 1 corresponds to lower velocity pressure within the plenum, due to the largest distance between the divider and the outlets (Delele et al., 2013). A decrease in the lateral distance between the divider and outlets leads to an increase in β-value. Thus, the β-value for outlets in row 2 (outlets 4–6), row 3 (Outlets 7–9), and row 4 (outlets 10–12) were 30.8, 44.9, and 20.2%, where the middle section of the air distributor (rows 2 and 3) outputs most of the air.

The comparison between the airflow data obtained from the in-field airflow measurements and the CFD airflow data,

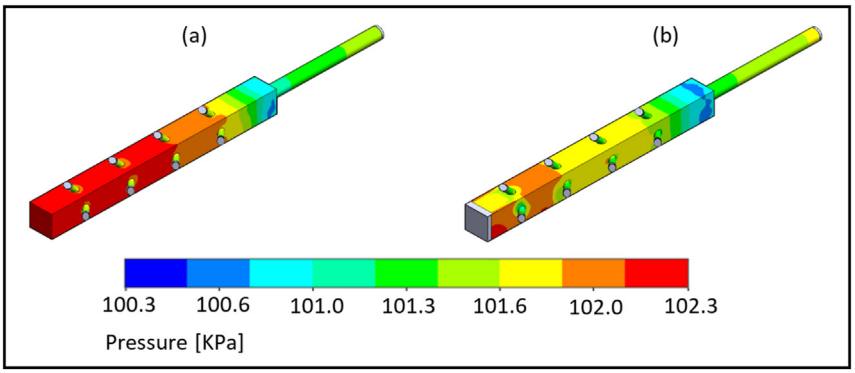

Fig. 3 – Surface plots showing pressure changes within the air distributor: (a) without divider, and (b) with divider.

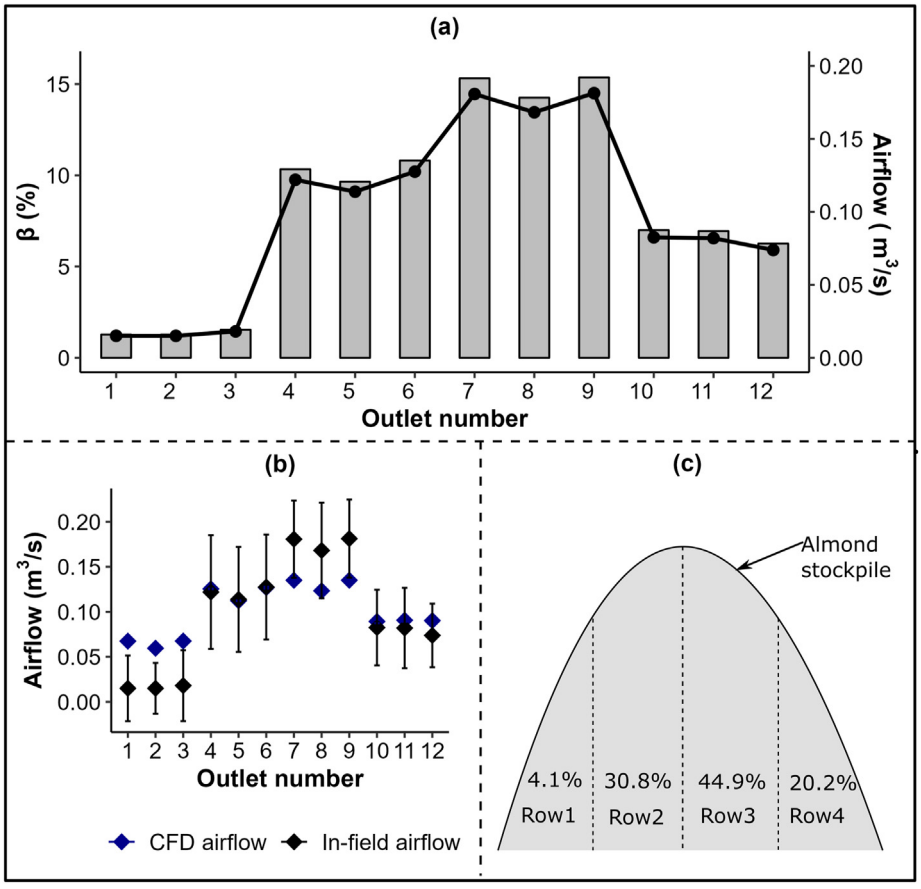

Fig. 4 – (a) Percentage airflow distribution (grey bars) and rate (black line); (b) airflow for CFD and in-field measurements; and (c) a schematic representation of an almond stockpile receiving air from an air distributor, with its corresponding β-values in the initial 4-row configuration, or when all the outlets are open. Error bars indicate standard deviation.

when all the outlets are open is shown in Fig. 4b. The mean RMSE% was equal to 31.2%. Even though high, the incongruity between the CFD model outputs and the in-field measurements can be attributed to iteration and grid convergence, discrepancies between the physical properties of the fabricated air distributor in comparison to the CFD model, and high variability of in-field measurements. Other CFD modelling studies have yielded a wide range of RMSE% rates, partly based on model complexity and environmental conditions that cannot be entirely included in the CFD design and simulation (Celik et al., 2007). On the low end (<10 RMSE%); Sonthikun et al. (2016) reported RMSE% between 2.3 and 5.9% when simulating the temperature and airflow distribution of a solar biomass dryer; Fohimi et al. (2020) predicted the air

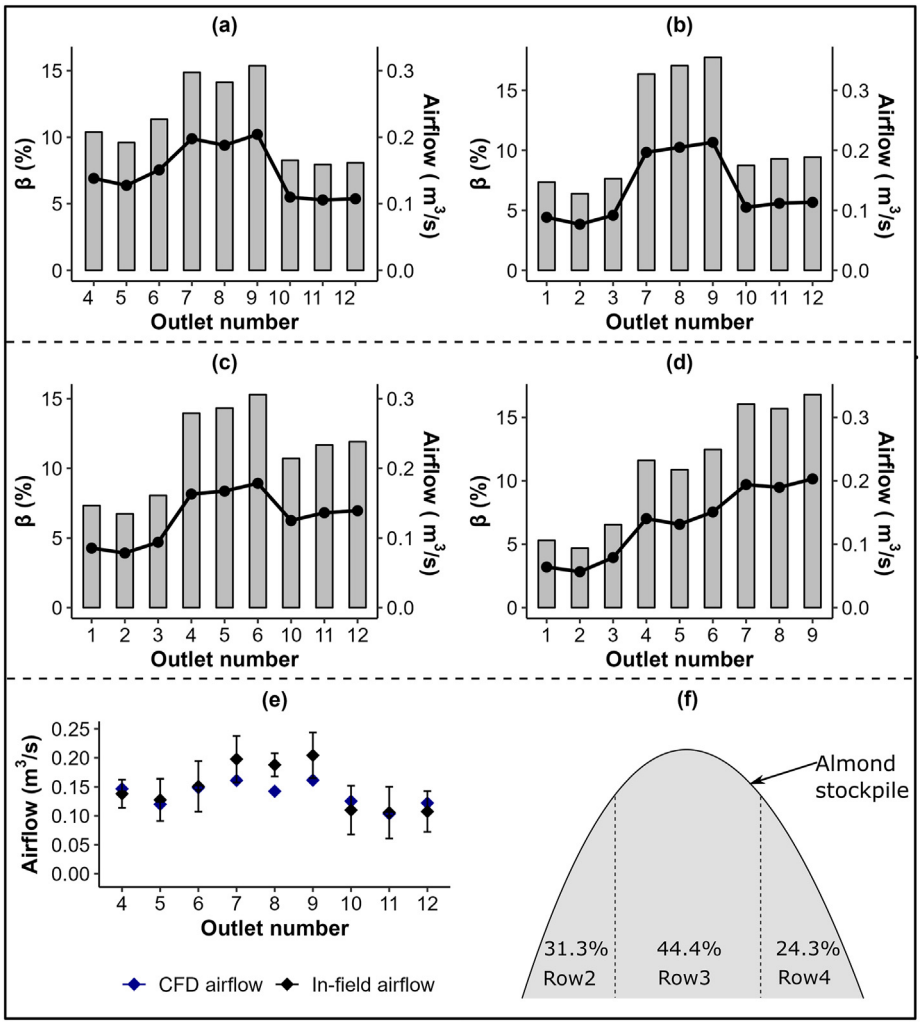

Fig. 5 – Percentage airflow distribution (gray bars) and airflow rate (black line) when sealing outlets in rows (a) 1; (b) 2; (c) 3; and (d) 4. (e) Airflow for CFD and in-field measurements; and (f) a schematic representation of an almond stockpile receiving air from an optimized 3-row air distributor design, with sealed outlets in row 1, with its corresponding β-values. Error bars indicate standard deviation.

ventilation and thermal comfort of an Atrium space with a RMSE% of less than 3%; Antony and Shyamkumar (2016) simulated the air velocity of a fluidized bed dryer with a RMSE% of between 4.7 and 8.23%; and Zhang et al. (2016) predicted the air temperature and velocities for aeration of an indoor plant factor system with RMSE% of 8.9% and 7.5%, respectively. Conversely, studies that reported high errors rates include; Ali et al.(2012) who predicted the velocity and temperature of a ship cabin air distributor with a RMSE% of 20.3% and 5.7%, respectively; Ameer et al.(2016) predicted air velocity distribution and ventilation effectiveness of wind towers with RMSE% of 1.58–24.3%; and Lawrence and Maier (2011) obtained RMSE% of 4.4% and 23.1% at the center and periphery, respectively for airflow distribution in a maize silo with different grain mass configurations.

In this study, the highest RMSE% was observed in the airflow outputs for row 1 (outlets 1–3). In addition, row 1 outlets also produced the least amount of airflow, as seen in Fig. 4c. Therefore, there was a need to optimize the design and explore the effect on air distribution with a 3-row, instead of a 4-row air configuration.

3.3. *Air distributor optimization and corresponding CFD air distributor model validation*

Figure 5 shows the air distributor in-field airflow measurement results (black line) and corresponding β-values (gray bars) when outlets in rows 1 (a), 2 (b), 3 (c), and 4 (d) were subsequently sealed. Sealing outlets in row 1 yielded the lowest airflow SD on the open outlets (0.03 $m^3 s^{-1}$), in comparison to sealing outlets in rows 2 (0.06 $m^3 s^{-1}$), 3 (0.04 m^3 s), and 4 (0.06 $m^3 s^{-1}$).

Comparison between the in-field measured airflows and the CFD-generated airflow data based on the optimized air distributor design with a 3-row configuration is shown in Fig. 5e. The mean RMSE% of the 3-row optimized design was equal to 14.72%, which is within an acceptable range in relation to other studies and lower than the 4-row design. In addition, the 3-row optimized air distributor delivers air

matching the natural shape of the stockpile, where most of the air is delivered to the middle section, or where the highest volume of almonds is located. The final implementation of the optimized 3-row air distributor can be performed in two ways: 1) Selectively sealing specific outlets; and 2) Strategic adjustments to the placement of the air distributor within the A-frame of the SHAD or placing the air distributor towards the entrance of the A-frame. Modifying the placement of the air distributor can easily ensure that the outlets in row 3, which deliver the highest airflow are positioned beneath the tallest section of the stockpile, and therefore outlets in rows 2 and 4 are positioned beneath the sections in the stockpile that contain less almonds, thus enhancing the effectiveness of air distribution. Ultimately, a 3-row configuration air distributor yielded β-values of 31.3, 44.4, and 24.3%, as seen in Fig. 5f.

4. Conclusions

This study focused on developing an air distribution system to enhance the performance of a previously developed SHAD. The addition of the air distributor aimed to optimize the efficiency of air distribution during the dehydration process of stockpiled almonds. In-field airflow measurements from the 12-outlet air distributor yielded β-values of 4.1, 30.8, 44.9, and 20.2% across outlets in rows 1, 2, 3, and 4, respectively. This uneven air distribution would likely affect the performance of the SHAD and therefore compromise the dehydration of almonds around the first row. As such, a 3-row air distributor was optimized through selective sealing of outlets in row 1, which yielded improved β-values of 31.3%, 44.4%, and 24.3% for rows 2, 3, and 4, respectively. The optimized 3-row air distributor configuration is desired, since the middle and tallest section of the stockpile, which contains the highest volume of almonds, will receive most of the airflow. Validation of the air distributor between the in-field airflow measurements and CFD airflow data showed that the RMSE% was 31.21% and 14.72% for the initial 4-row air distributor configuration, and the optimized 3-row configuration (i.e. sealed outlets in row 1), respectively. Comparison with similar studies revealed that the RMSE% of the 4-configuration model is beyond limits, but the optimized 3-configuration model is within acceptable limits.

The optimized 3-row air distributor configuration that emerged from this study appears to be a promising addition to increase air distribution capability of the SHAD and increase its drying performance. Future work will explore an air distributor design with an increased overall length for larger stockpiles, but based on the observation here, the overall concept and design should not significantly change. Part 2 of this study explores the air distributor applicability in combination with the SHAD with the purpose of effectively dehydrating almonds, while maintaining their quality, in different stockpile sizes (Mayanja et al., 2023).

Declaration of competing interest

The authors declare that they have no known competing financial interests or personal relationships that could have appeared to influence the work reported in this paper.

Acknowledgments

This work was financially supported by the Almond Board of California (Grant number: HARV1A).

REFERENCES

Ali, A. A., Elsafty, A. F., & Elsayed, A. A. (2012). CFD Investigation of indoor air distribution in marine applications. *European Journal of Scientific Research, 88*(2), 196–208.

Ameer, S. A., Chaudhry, H. N., & Agha, A. (2016). Influence of roof topology on the air distribution and ventilation effectiveness of wind towers. *Energy and Buildings, 130*, 733–746. https://doi.org/10.1016/j.enbuild.2016.09.005

Antony, J., & Shyamkumar, M. B. (2016). Study on sand particles drying in a fluidized bed dryer using CFD. *International Journal of Engineering, 8*(2), 129–145.

Awbi, H. B. (1998). Energy efficient room air distribution. *Renewable Energy, 15*(1–4), 293–299. https://doi.org/10.1016/S0960-1481(98)00176-1

Camilleri, R., Howey, D. A., & Mcculloch, M. D. (2015). Predicting the flow distribution in compact parallel flow heat exchangers. *Applied Thermal Engineering, 90*, 551–558. https://doi.org/10.1016/j.applthermaleng.2015.07.002

CARB. (2017). *Agricultural harvest operations. California air resources board: Emission inventory source category*. Retrieved from https://ww3.arb.ca.gov/ei/areasrc/fullpdf/full7-5_2017.pdf.

Celik, I., Karaismail, E., & Parsons, D. (2007). *A reliable error estimation technique for CFD applications*. Retrieved from. Paper presented at AVT-147 Symposium on Computational Uncertainty in Military Vehicle Design, Neuilly-sur-Seine, France https://www.sto.nato.int/publications/STO%20Meeting%20Proceedings/RTO-MP-AVT-147/MP-AVT-147-32.pdf.

Cengel, Y. A., & Cimbala, J. M. (2017). *Fluid mechanics: Fundamentals and applications* (4th ed.). New York, NY, USA: McGraw-Hill Higher Education (Chapter 10)).

Colak, N., & Hepbasli, A. (2007). Performance analysis of drying of green olive in a tray dryer. *Journal of Food Engineering, 80*(4), 1188–1193. https://doi.org/10.1016/j.jfoodeng.2006.09.017

Daly, A. (2002). Underfloor air distribution: Lessons learned. *ASHRAE Journal, 44*(5), 21–24.

Delele, M. A., Ngcobo, M. E. K., Getahun, S. T., Chen, L., Mellmann, J., & Opara, U. L. (2013). Studying airflow and heat transfer characteristics of a horticultural produce packaging system using a 3-D CFD model. Part II: Effect of package design. *Postharvest Biology and Technology, 86*, 546–555. https://doi.org/10.1016/j.postharvbio.2013.08.015

Depypere, F., Pieters, J. G., & Dewettinck, K. (2004). CFD analysis of air distribution in fluidised bed equipment. *Powder Technology, 145*(3), 176–189. https://doi.org/10.1016/j.powtec.2004.06.005

Dickerson, R. E., Gray, H. B., & Haight, G. P. (1979). *Chemical principles* (3rd ed.). Menlo Park, CA, USA: The Benjamin/Cummings Publishing Company, Inc.

Downey, D., Giles, D. K., & Thompson, J. F. (2008). In situ transmissometer measurements for real-time monitoring of dust discharge during orchard nut harvesting. *Journal of Environmental Quality, 37*(2), 574–581. https://doi.org/10.2134/jeq2006.0423

Drazin, P. G., & Riley, N. (2006). *The Navier-Stokes equations: A classification of flows and exact solutions* (Vol. 334). New York, USA: Cambridge University Press.

Fohimi, N. A. M., Asror, M. H., Rabilah, R., Mohammud, M. M., Ismail, M. F., & Ani, F. N. (2020). CFD simulation on ventilation of an indoor Atrium space. *CFD Letters, 12*(5), 52–59.

Goldhamer, D. A., & Viveros, M. (2002). Effects of preharvest irrigation cutoff durations and postharvest water deprivation on almond tree performance. *Irrigation Science, 19*(3), 125–131. https://doi.org/10.1007/s002710000013

Hassan, J. M., Mohamed, T. A., Mohammed, W. S., & Alawee, W. H. (2014). Modeling the uniformity of manifold with various configurations. *Journal of Fluids*, 1–8. https://doi.org/10.1155/2014/325259

Hassan, J. M., Mohamed, T. A., Mohammed, W. S., & Alawee, W. H. (2015). Experimental and numerical study on the improvement of uniformity flow for three-lateral dividing manifold. *International Journal of Engineering and Technology, 12*(1), 29–37.

IRRI. (2021). *International rice research institute*. Retrieved from. Rice Knowledge Bank. Air Distribution System http://www.knowledgebank.irri.org/step-by-step-production/postharvest/drying/dryer-components/item/air-distribution-system.

Jones, W. P. (2019). *Air distribution. Air conditioning applications and design* (2nd ed.). New York, NY, USA: Butterworth-Heinemann.

Lawrence, J., & Maier, D. E. (2011). Three-dimensional airflow distribution in a maize silo with peaked, levelled and cored grain mass configurations. *Biosystems Engineering, 110*(3), 321–329. https://doi.org/10.1016/j.biosystemseng.2011.09.005

Lee, M., Park, G., Park, C., & Kim, C. (2020). Improvement of grid independence test for computational fluid dynamics model of building based on grid resolution. *Advances in Civil Engineering, 2020*, 1–11. https://doi.org/10.1155/2020/8827936

Leys, C., Ley, C., Klein, O., Bernard, P., & Licata, L. (2013). Detecting outliers: Do not use standard deviation around the mean, use absolute deviation around the median. *Journal of Experimental Social Psychology, 49*(4), 764–766. https://doi.org/10.1016/j.jesp.2013.03.013

Lin, Z., Chow, T. T., Tsang, C. F., Fong, K. F., & Chan, L. S. (2005). CFD study on effect of the air supply location on the performance of the displacement ventilation system. *Building and Environment, 40*(8), 1051–1067. https://doi.org/10.1016/j.buildenv.2004.09.003

Martha, A. K., Harbir, K., Luxin, W., Michelle, D. D., & Linda, J. H. (2012). Survival of Salmonella, Escherichia coli O157:H7, and Listeria monocytogenes on inoculated almonds and pistachios stored at −19, 4, and 24°C. *Journal of Food Protection, 75*(8), 1394–1403. https://doi.org/10.4315/0362-028X.JFP-12-023

Matsson, J. (2012). *An introduction to SOLIDWORKS flow simulation 2012. SDC publications*. Mission, KS, USA: SDC Publications.

Mayanja, I. K., Coates, M. C., Niederholzer, F., & Donis-González, I. R. (2021). Development of a stockpile heated and ambient air dryer (SHAD) for freshly harvested almonds. *Applied Engineering in Agriculture, 37*(3), 417–425. https://doi.org/10.13031/aea.14364

Mayanja, I. K., Coates, M. C., Niederholzer, F., & Donis-González, I. R. (2023). Dryer (SHAD) with an air distributor – Part 2. In *Drying of freshly harvested almonds using a Stockpile Heated and ambient Air* [Submitted for publication].

Nielsen, P. V. (2015). Fifty years of CFD for room air distribution. *Building and Environment, 91*, 78–90. https://doi.org/10.1016/j.buildenv.2015.02.035

Riveros, H. G., & Riveros-Rosas, D. (2010). Laminar and turbulent flow in water. *Physics Education, 45*(3), 288–291. https://doi.org/10.1088/0031-9120/45/3/010

Royapoor, M., & Roskilly, T. (2015). Building model calibration using energy and environmental data. *Energy and buildings, 94*, 109–120. https://doi.org/10.1016/j.enbuild.2015.02.050

RSES. (2008). *Refrigeration Service engineers society. The principles of air flow, air pressure, and air filtration*. Retrieved from. National Air Filtration Association http://www.rses.org/assets/serviceapplicationmanual/630-156.pdf.

Schatzki, T. F., & Ong, M. S. (2001). Dependence of aflatoxin in almonds on the type and amount of insect damage. *Journal of Agricultural and Food Chemistry, 49*(9), 4513–4519. https://doi.org/10.1021/jf010585w

Sonthikun, S., Chairat, P., Fardsin, K., Kirirat, P., Kumar, A., & Tekasakul, P. (2016). Computational fluid dynamic analysis of innovative design of solar-biomass hybrid dryer: An experimental validation. *Renewable Energy, 92*, 185–191. https://doi.org/10.1016/j.renene.2016.01.095

Tórrez, N., Gustafsson, M., Schreil, A., & Martínez, J. (1998). Modeling and simulation of crossflow moving bed grain dryers. *Drying Technology, 16*(9–10), 1999–2015. https://doi.org/10.1080/0737393980891750

Versteeg, H. K., & Malalasekera, W. (2007). *An introduction to computational fluid dynamics: The finite volume method* (2nd ed.). Harlow, England: Pearson Education Ltd.

Wang, C. C., Yang, K. S., Tsai, J. S., & Chen, I. Y. (2011). Characteristics of flow distribution in compact parallel flow heat exchangers, part I: Typical inlet header. *Applied Thermal Engineering, 31*(16), 3226–3234. https://doi.org/10.1016/j.applthermaleng.2011.06.004

Wan, X., Wang, W., Liu, J., & Tong, T. (2014). Estimating the sample mean and standard deviation from the sample size, median, range and/or interquartile range. *BMC Medical Research Methodology, 14*(1), 135. https://doi.org/10.1186/1471-2288-14-135

Zhang, Y., Kacira, M., & An, L. (2016). A CFD study on improving air flow uniformity in indoor plant factory system. *Biosystems Engineering, 147*, 193–205. https://doi.org/10.1016/j.biosystemseng.2016.04.012

Zhou, P., Wu, B., Hu, Y., Zheng, D., Fleitz, J., Trajkovski, R., & Zhou, C. Q. (2009). CFD study for air distribution in hydrogen reformer furnace. In *Paper presented at in heat transfer summer conference*. USA: San Francisco, CA. https://doi.org/10.1115/HT2009-88620.